G&G
Gem News International

Contributing Editors
Emmanuel Fritsch, *University of Nantes, CNRS, Team 6502, Institut des Matériaux Jean Rouxel (IMN), Nantes, France* (fritsch@cnrs-imn.fr)
Gagan Choudhary, *Gem Testing Laboratory, Jaipur, India* (gagan@gjepcindia.com)
Christopher M. Breeding, *GIA, Carlsbad* (christopher.breeding@gia.edu)

COLORED STONES AND ORGANIC MATERIALS

Sapphires from northern Ethiopia. Since February 2017, rumors of a newly discovered sapphire deposit in northern Ethiopia have been circulating in the trade. In June, one of the authors (SB-L) visited the mining area, located in the country's Tigray region. The city of Aksum (or Axum), about 35 km south of the Eritrean border, is used as a base for gem merchants. Mining and trading is concentrated around the town of Chila, about 25 km northwest of Aksum. Based on the literature, the alkali basalt field that produces the sapphire stretches into Eritrea, although no sapphires from that area have reached the market. Several sites are active, and about 5,000 miners were working the deposits. All of the deposits are secondary in nature and have yielded rounded crystals. The majority of the rough (figure 1) weighs 2–3 grams, but crystals over 50 g have been reported; the larger ones are usually cracked. Heat treatment experiments are being conducted in Chanthaburi (Thailand) and Beruwala (Sri Lanka) to see how the material reacts. It is estimated that 5–10% of the sapphires do not require heat treatment.

At the end of April, the first parcels started to arrive in Bangkok, and GIA was able to study selected samples donated by author SB-L. The color of the crystals ranged from dark to light blue, and many contained fine rutile particles. Some stones had a trapiche-like pattern. The stones occasionally exhibited a green or yellow color, sometimes combined with blue in bicolor sapphires. All of the sapphires studied by GIA showed strong blue-green pleochroism. The main inclusions were intersecting twinning planes (figure 2), along with crystals, fingerprints, tubules, and bands of rutile particles (figure 3).

Editors' note: Interested contributors should send information and illustrations to Stuart Overlin at soverlin@gia.edu or GIA, The Robert Mouawad Campus, 5345 Armada Drive, Carlsbad, CA 92008.

Gems & Gemology, Vol. 53, No. 2, pp. 247–260.

Trace-element analysis using laser ablation–inductively coupled plasma–mass spectrometry (LA-ICP-MS) was performed on two samples. On each stone we measured 12 spots: six in a clean area and six in a particle-rich area. The clean areas from both stones showed very similar chemical composition, and the same was observed for the particle-rich areas. The compositional ranges of both stones, presented in table 1, clearly show that the chemical concentrations are different between the clean and particle-rich areas. None of the areas contained enough natural Be or Cr to detect with LA-ICP-MS. All samples showed a high Fe concentration. While Ti content was higher than Mg concentration in both areas, the particle-rich areas showed elevated levels of titanium (table 1). The UV-Vis-NIR spectrum shows a broad band around 860 nm, which is typical of basalt-related sapphires (figure 4).

Figure 1. Rough sapphires from a new deposit near Chila, Ethiopia. Photo by Simon Bruce-Lockhart.

TABLE 1. Chemical composition (ppma) of Ethiopian sapphire, obtained by LA-ICP-MS[a].

	^{24}Mg	^{47}Ti	^{51}V	^{57}Fe	^{69}Ga
Clean area	8–9	10–12	0.7–1.0	1362–1450	58–66
Particle-rich area	11–14	15–43	0.6–0.8	1365–1588	57–64

[a] *In total, 12 spots in clean areas and 12 in particle-rich areas were analyzed. Be and Cr were both below detection limit (0.2 and 0.4 ppma, respectively).*

Starting in May, many Sri Lankan dealers have traveled to Ethiopia to buy this material, causing steep price increases in local gem markets. All of the mining around Chila is artisanal, but large volumes of sapphire have been mined in a short time span. Time, and the results of the heat treatments, will show the viability of this deposit.

Wim Vertriest, Vararut Weeramonkhonlert, and Victoria Raynaud
GIA, Bangkok

Simon Bruce-Lockhart
Chanthaburi, Thailand

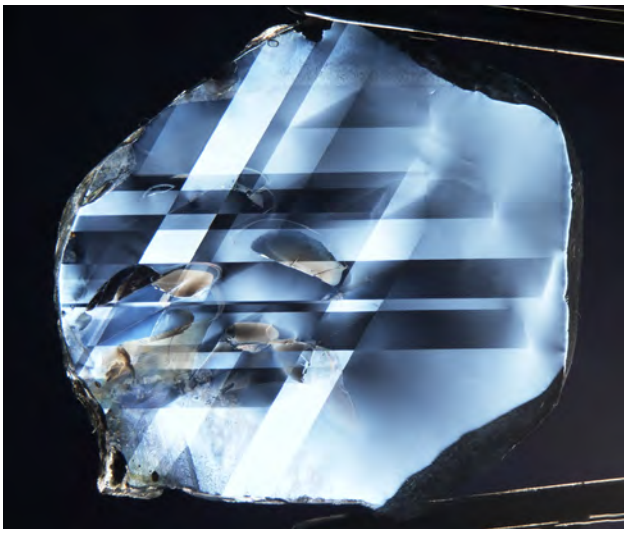

Figure 2. An Ethiopian sapphire wafer with two polished windows perpendicular to the c-axis under crossed polarizers shows two sets of twinning planes. Photo by Victoria Raynaud; field of view 13.4 mm.

New deposits of gem-quality common opal from Michoacán, Mexico. The principal gemological characteristic of precious opal is the play-of-color produced by the diffraction of white light from three-dimensionally stacked layers of microscopic spheres of silica. In comparison, so-called common opal does not show play-of-color but may be valued for its attractive bodycolors. Most play-of-color opals are opal-A (e.g., Australian and Brazilian sedimentary opal), which is amorphous in X-ray diffraction (XRD). Less-studied Mexican volcanic opals, both precious and common, are by contrast opal-CT (for "cristobalite-tridymite"). In these specimens, XRD shows diffraction peaks for highly disordered cristobalite with abundant tridymite stacking (M. Ostrooumov et al., "Spectres Raman des opales: aspect diagnostique et aide a la classification," *European Journal of Mineralogy*, Vol. 11, No. 5, 1999, pp. 899–908). Yet there have been few studies of gemological interest on the microstructure of common opals.

Recently, the author discovered new deposits of common gem opal (figure 5) in the hills near Lake Cuitzeo, in Mexico's Michoacán State. These opals were embedded in volcanic andesitic rocks. They were generally characterized by a medium to light orange to brown color, with no visible inclusions. While these new deposits are considered "common opal" since the material does not show play-of color, some gemologists may also consider the specimens to be fire opal due to the orangy bodycolor. The samples were studied at the Institute of Earth Sciences at the University of Michoacán in Morelia.

Standard gemological testing yielded refractive indices between 1.440 and 1.457 and hydrostatic specific gravities (SGs) ranging from 2.11 to 2.14. The material was inert to both long- and short-wave UV radiation. These properties suggested common opal, which we later confirmed with scanning electron microscopy (SEM), transmission electron

Figure 3. Left: An unidentified crystal surrounded by a fingerprint. Many particles and fine wispy fingerprints can be seen throughout the stone in darkfield lighting. Center: Intersection tubules associated with different types of fingerprints, shown here in fiber-optic lighting, were always found in the twinning planes of the Ethiopian sapphires. Right: Bands of particles seen with fiber-optic lighting. Photomicrographs by Victoria Raynaud; fields of view 1.20 mm (left), 3.60 mm (center), and 1.44 mm (right).

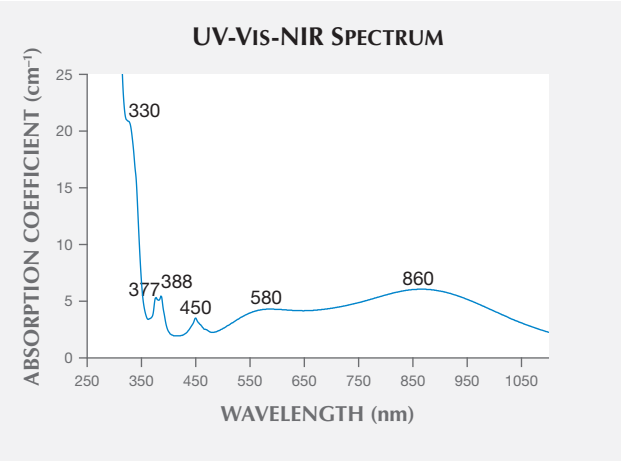

Figure 4. UV-Vis-NIR spectrum of the o-ray of a greenish blue Ethiopian sapphire. Optical path length 1.13 mm.

Figure 6. SEM image of the heterogeneous nanostructure of a common gem opal from the Cuitzeo area in Michoacán. The spheres are too small, irregularly sized, and disorganized to exhibit play-of-color.

microscopy (TEM), atomic force microscopy (AFM), Raman microprobe, and infrared spectroscopy.

Previous research (E. Fritsch et al., "Mexican gem opals: Nano-and micro-structure, origin of colour, comparison with other common opals of gemmological significance," *Australian Gemmologist*, Vol. 21, No. 6, 2002, pp. 230–233) has shown that Mexican opals with play-of-color exhibit a higher degree of organization. In these specimens, nanoparticles measuring about 10–50 nm in diameter form pseudospheres (lepispheres) of appropriate size to diffract visible light (about 200 nm) in a matrix of less acid-soluble silica particles. When examined with a scanning electron microscope, fresh broken surfaces show no particular organization, but after etching with diluted hydrofluoric acid (10% vol. HF), the microscopic arrangement of spheres is revealed. There is a continuum of structures between opals with and without play-of color. In addition to the role of particle size, rounder spheres with a more organized structure display a more noticeable play-of-color with a wider range of colors.

Figure 5. Gem-quality common opal was recently discovered in Michoacán State in western central Mexico. The approximate size of this sample is 15.04 × 7.68 × 5.57 cm. Photo by M. Ostrooumov.

From SEM and AFM images, it is clear that these newly discovered common opals from Michoacán are built from a random aggregation of small, near-spherical grains, averaging 60 to 100 nm in size. (The software we used was ImageJ, an open-source image processing program designed to generate scientific multidimensional images.) The apparent diameter of some grains actually ranges from about 120 to 130 nm (figures 6 and 7). The nanostructure of this common opal explains the absence of play-of-color. In this case, we can consider the following general explanations for the lack of play-of-color:

1. The spheres do not have the same size (heterogeneous structure).
2. The spheres are not perfectly spherical.
3. The spheres are the same size but not well organized.
4. The spheres are too small (<150 nm) or too large (>300 nm) to diffract light.

In some cases two or more of these conditions occur in the same sample.

All Mexican volcanic CT-opals have similar Raman spectra characterized by a very strong general band (apparent maximum toward 325 cm^{-1}) that shows a complex structure with lines of weak to medium intensity (M. Ostrooumov et al., "Spectres Raman des opales: aspect diagnostique et aide a la classification," *European Journal of Mineralogy*, Vol. 11, No. 5, 1999, pp. 899–908). According to theoretical calculations, the normal modes in the 300–350 cm^{-1} range consist mainly of Si-O-Si bending vibrations

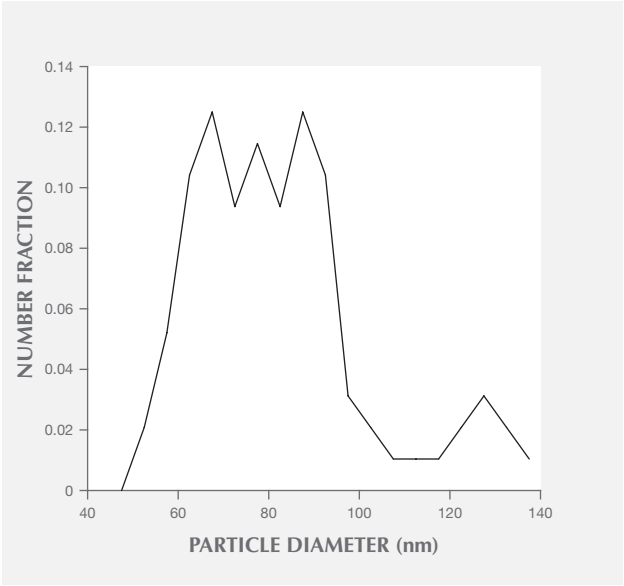

Figure 7. Distribution of particle sphere diameters in the nanostructure of the newly discovered Mexican volcanic opal. Most of the spheres are 60–100 nm, a size too small to diffract light.

of ring atoms. Other principal bands in the Raman spectra of opal from these new deposits are found at about 800 and 960 cm^{-1}, 1069–1086 cm^{-1}, and 1600 and 3200 cm^{-1}. These bands belong to α-tridymite, α-cristobalite, α-quartz, and groups of H_2O and OH.

Infrared absorption bands were observed between 4000 and 400 cm^{-1}, which is typical for all varieties of micro- and non-crystalline opals (C, CT, and A). The three strong bands near 1100, 790, and 480 cm^{-1} are common to all silicates with tetrahedrally coordinated silicon (M. Ostrooumov, "A Raman, infrared and XRD analysis of the instability in volcanic opal from Mexico," *Spectrochimica Acta, Part A*, Vol. 68, No. 4, 2007, pp. 1070–1076). Broadly speaking, in opal-CT only localized Si-O-Si stretching and bending vibrations remain. The distinction between opal-CT and opal-A requires careful inspection of the frequencies of the three strong Si-O bands. In particular, the band at 790 cm^{-1} is always at higher frequency in opal-A than in opal-CT. Broad absorption bands between 3700 and 2700 cm^{-1} are due to fundamental O-H stretching vibrations. For example, a very broad band is present at around 3448–3458 cm^{-1}, with a shoulder at about 3250 cm^{-1} that is generally considered to be related to hydrogen-bonded molecules of water.

Based on TEM results, we have been able to prove that the orange to brown bodycolor of Mexican common opal is due to nano-inclusions of an iron-containing material. It is probably related to hematite, which is often found associated with common opal in nodules. It typically appears as needles measuring 10 to 20 nm wide by 100 to 200 nm long, seen only with TEM.

Mikhail Ostrooumov (ostroum@umich.mx)
University of Michoacán, Institute of Earth Sciences
Morelia, Michoacán, Mexico

Raspberry-red garnet with black core. Raspberry-red grossular garnet mineral specimens have been popular in the collector market since their discovery in 1994 in the Sierra de Cruces range in the State of Coahuila, Mexico. V.W. Lueth and R. Jones ("Red grossular from the Sierra de Cruces, Coahuila, Mexico," *Mineralogical Record*, Vol. 34, No. 6, 2003, p. 73) described the geological environment where the garnet was discovered and the petrological composition of the garnet and matrix (figure 8). An interesting internal characteristic of this type of grossular crystal is its raspberry-red rim and black core with sharp color transition at the core-rim boundary. Lueth and Jones reported that the raspberry-red rim is composed mainly of grossular and the black core contains up to 4.5 wt.% titanium that can be used to calculate additional morimotoite and schorlomite garnet end-member species (table 2). No detailed chemical analysis of the black core was presented, however. To better understand the composition of this type of garnet, we prepared a thin section sliced from the middle of one garnet crystal (see the color-zoned image in

TABLE 2. Cation site occupancies for garnet end members.

End members		Cation site			Anion site
		Dodecahedral	Octahedral	Tetrahedral	
Schorlomite	Schorlomite	Ca_3	Ti_2	Si, Fe^{3+}_2	O_{12}
	Schorlomite-Al	Ca_3	Ti_2	Si, Al_2	O_{12}
Morimotoite	Morimotoite	Ca_3	Ti, Fe^{2+}	Si_3	O_{12}
	Morimotoite-Mg	Ca_3	Ti, Mg	Si_3	O_{12}
	Morimotoite-Fe	Fe^{2+}_3	Ti, Fe^{2+}	Si_3	O_{12}
Grandite	Grossular	Ca_3	Al_2	Si_3	O_{12}
	Andradite	Ca_3	Fe^{3+}_2	Si_3	O_{12}
Kimzeyite	Kimzeyite	Ca_3	Zr_2	$SiAl_2$	O_{12}
	Kimzeyite-Fe	Ca_3	Zr_2	$SiFe^{3+}_2$	O_{12}

Figure 8. A very fine 4.5 × 3.1 × 2.1 cm specimen of raspberry-red grossular from skarn deposits, with crystals approaching 1 cm. The matrix consists of calcite, quartz, wollastonite, and scapolite. Photo by Kevin Schumacher.

the middle of figure 9) for detailed chemical analysis at GIA's Carlsbad laboratory.

The section's chemical composition was obtained with a Thermo Fisher iCAP Q ICP-MS coupled with a New Wave Research UP-213 laser ablation unit. ^{29}Si was used as the internal standard. GSD-1G and GSE-1G were used as external standards. A line of 33 ablation spots was selected to cross the whole section from one outer rim to the opposite outer rim. The black core contained up to 27.91 mol.% morimotoite and up to 4.07 mol.% schorlomite (figure 9). The detailed composition of the black core of spot 7 to spot 15 (the light blue vertical zone in figure 9) is listed in table 3. The black core contained 4.10–5.04 wt.% TiO_2, confirming the analytical results reported by Lueth and Jones, and 4.42–5.49 wt.% FeO_{tot}. It also contained 0.26–0.84 wt.% ZrO_2 that could be used to calculate a distinct kimzeyite garnet end-member species (tables 2 and 3; table 2 gives the composition and site occupancy of the end members). It is the first time a detailed chemical analysis of the black core of this type of raspberry-red garnet has been documented.

Ziyin Sun and Nathan D. Renfro
GIA, Carlsbad

"Sango pearl" from Japan. A type of pink Japanese akoya cultured pearl, introduced about a decade ago and known as "Sango" pearl (figure 10), uses a pink coral nucleus and a *Pinctada fucata* mollusk. It is produced by Matsumoto Pearls, a Japanese pearl farming company based in Uwajima, Ehime Prefecture. *Sango* is the Japanese word for coral, and the species of pink coral used as the nucleus is likely a *Corallium* species, one of the precious corals harvested off the Pacific coast of Japan, especially around southern Kochi Prefecture (N. Iwasaki et al., "Biology of Japanese *Corallium* and *Paracorallium*," *Proceedings of the First International Workshop on Corallium Science, Management, and Trade*, 2009, pp. 68–70). Matsumoto Pearls has successfully combined two beautiful organic gem materials to produce these attractive pink-colored pearls.

The coral nuclei in this study exhibited a pinkish orange color and measured 5.60–5.90 mm in diameter. Under microscopic examination, white layer-like structures and banding as well as polyp-related cavities have sometimes been

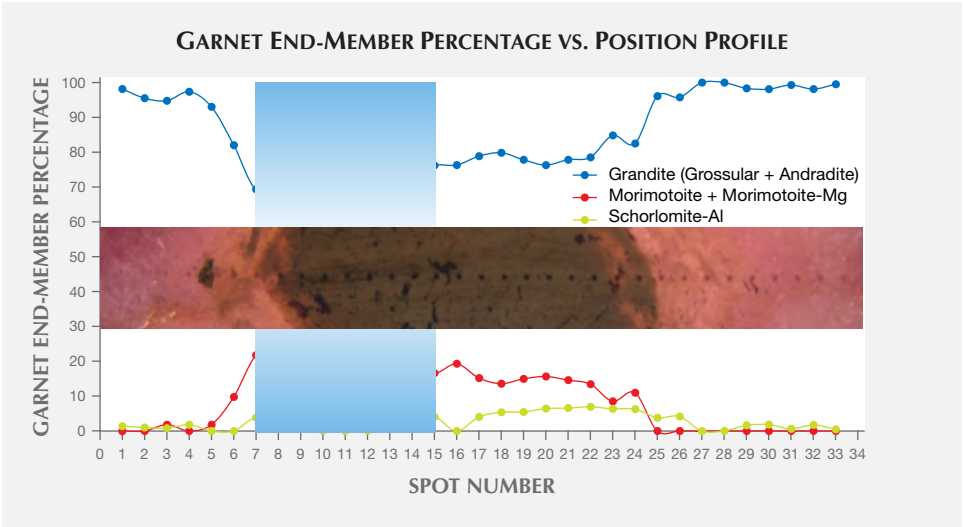

Figure 9. Garnet end-member percentage vs. position profile revealed that the black core of the garnet was rich in morimotoite and schorlomite. The pink rim of the garnet was composed almost entirely of grossular with minor andradite.

TABLE 3. Chemical composition of grandite-morimotoite garnet spots by LA-ICP-MS.

Number of spots	spot 7	spot 8	spot 9	spot 10	spot 11	spot 12	spot 13	spot 14	spot 15
					wt.% oxides				
MgO	1.37	1.13	1.37	1.38	1.32	1.28	1.23	1.23	1.30
Al_2O_3	14.84	14.88	15.48	15.21	15.32	15.30	15.77	15.34	15.85
SiO_2	37.28	38.31	37.86	38.67	38.95	38.71	38.26	37.64	37.69
CaO	34.89	35.99	35.29	34.94	34.20	35.11	35.39	35.23	35.55
TiO_2	5.04	4.28	4.80	4.57	4.80	4.17	4.10	4.51	4.29
V_2O_3	0.02	0.02	0.02	0.02	0.02	0.02	0.02	0.02	0.02
Cr_2O_3	0.02	0.01	0.00	0.00	0.00	0.00	0.00	0.00	0.00
MnO	0.10	0.13	0.14	0.15	0.15	0.16	0.15	0.14	0.15
FeO_{tot}	5.49	4.42	4.62	4.60	4.59	4.81	4.75	5.09	4.66
ZrO_2	0.84	0.73	0.35	0.40	0.57	0.37	0.26	0.71	0.42
Total	99.89	99.90	99.93	99.93	99.92	99.93	99.93	99.91	99.93
					mol.% end members				
Kimzeyite	1.59	1.37	0.66	0.75	0.00	0.70	0.48	1.33	0.79
Schorlomite-Al	3.78	0.59	3.37	0.10	0.00	0.07	2.27	3.08	4.07
Morimotoite	15.21	11.36	12.62	20.55	27.91	18.14	12.15	12.90	7.33
Morimotoite-Mg	6.56	12.08	8.35	5.64	0.00	5.80	6.97	7.05	9.27
Goldmanite	0.05	0.05	0.06	0.06	0.06	0.05	0.05	0.06	0.06
Uvarovite	0.05	0.03	0.00	0.00	0.01	0.00	0.00	0.01	0.00
Spessartine	0.23	0.29	0.31	0.33	0.32	0.34	0.33	0.31	0.33
Pyrope	3.08	0.33	2.48	3.41	3.66	2.98	2.38	2.37	1.89
Almandine	0.00	0.00	0.00	0.00	0.52	0.00	0.00	0.00	0.00
Grossular	59.13	65.13	63.47	64.50	65.28	65.36	66.02	62.75	64.82
Andradite	10.19	8.59	8.57	4.56	0.00	6.44	9.22	10.01	11.33
Remainder[a]	0.06	0.06	0.06	0.05	1.19	0.06	0.07	0.06	0.05
Total	99.93	99.88	99.95	99.95	98.95	99.94	99.94	99.93	99.94

[a]*The "remainder" in the end-member components is what is left over after assigning all the atoms to stoichiometric garnet formula. This value is related to analytical error in the chemical measurements.*

observed. The nuclei also exhibit a weak whitish and stronger whitish fluorescence under short-wave and long-wave UV, respectively. The coral bead's Raman spectrum (figure 11, top) shows strong pigment peaks at 1129 and 1517 cm^{-1} and calcite peaks (e.g., 280 and 713 cm^{-1}), identifying them as *Corallium* species, as in S. Karampelas et al. ("Identification of the endangered pink-to-red *Stylaster* corals by Raman spectroscopy," Spring 2009 *G&G*, pp. 48–52). The full-range photoluminescence spectra closely match that of natural pink coral with natural pigment-related peaks, similar to those in C.P. Smith et al. ("Pink-to-red coral: A guide to determining origin of color," Spring 2007 *G&G*, pp. 4–15). Visible-range reflectance spectra (figure 11, middle) reveal peaks at 468, 482, 590, and 666 nm, like those observed in the spectra of natural coral by C.P. Smith et al. (2007).

Figure 10. Sango pearls (left and center) and a coral bead nucleus (right), each approximately 6 mm in diameter. Photo by Y. Katsurada.

Ten partially drilled Sango pearls examined for this note were of a similar size (5.60–6.00 mm) as the coral beads used as nuclei. No color concentrations were noted down the drill holes or anywhere on their nacreous surfaces using a loupe or microscope. The nacre thickness measured between 120 and 400 microns (0.12–0.40 mm) under the microscope

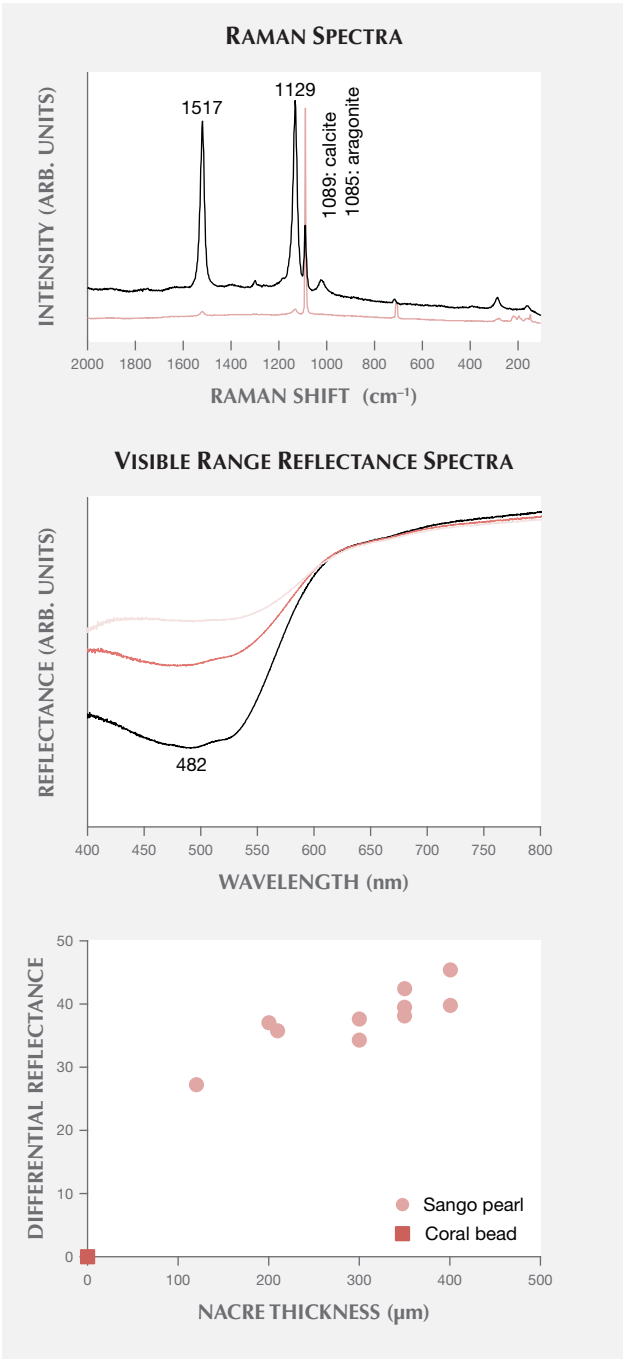

Figure 11. Top: Raman spectra of a coral bead (black trace) and a Sango cultured pearl (pink trace) with pigment-related peaks at 1129 and 1517 cm^{-1}. The bead's peaks are stronger at those wavelengths. Middle: Visible-NIR spectra of a coral bead (black trace) and two Sango cultured pearls showing the different reflectance values obtained. The dark pink trace represents thinner nacre (120 µm thick); the light pink trace is from nacre that is 400 µm thick. Bottom: Plot of the relationship between nacre thickness and the differential reflectance of Sango pearls at 482 nm based on the average reflectance of the coral beads (differential reflectance = $R_{Sango\ pearls} - R_{coral\ beads}$).

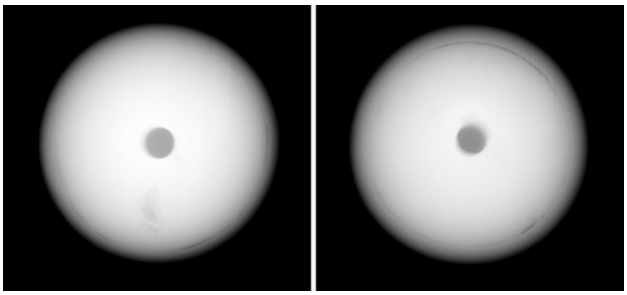

Figure 12. RTX images of Sango cultured pearls showing clear demarcations between the larger coral bead nucleus and thinner nacre overgrowth. The pearl on the left has a thinner nacre than the one on the right.

using a small table gauge. The different nacre thicknesses were also visible in real-time X-ray (RTX) images (figure 12). The pearls exhibited excellent luster, with almost no overtone and very weak orient, and showed a weak yellow to greenish yellow fluorescence under long-wave and short-wave UV radiation, respectively. These observations indicated that the 10 samples' pink coloration was natural, though it remained to be seen whether the pink color originated from the pearls' nacre or the underlying coral beads.

Chemical analysis using an energy-dispersive X-ray fluorescence (EDXRF) spectrometer revealed manganese levels of 0 to 28 ppmw and strontium levels of 1077 to 1719 ppmw, indicating that the pearls formed in a saltwater environment. A useful observation was that pearl color seemed to be related to nacre thicknesses: Thin nacre overgrowth produced a more obvious pink tint, while thicker nacre resulted in a less saturated pink. Likewise, the Raman and visible-range reflectance spectra were also related to the nacre thickness. Raman spectra for pearls with thin nacre showed stronger pigment peaks at approximately 1129 and 1517 cm^{-1}, similar in strength to those noted in the coral beads; only the aragonite-related peaks—and no pigment peaks—were noted in pearls with thicker nacre (see figure 11, top). The visible-range spectra of the pearls possessing thin nacre also matched the coral beads more closely, albeit with a lower reflectance (figure 11, middle), while pearls with thicker nacre had higher reflectance, as would be expected for lighter-colored pearls. By correlating the coral pigments with the maximum visible reflectance spectrum at 482 nm, the point of least reflectance (see figure 11, bottom), the relationship between nacre thickness and the visible spectra of the pearls could be gauged. The intensity at 482 nm indicates that the pink color of Sango pearls most likely originates from their coral nuclei.

While Sango pearls are not the first cultured pearls to use atypical bead nuclei in the form of other gem materials (see K. Scarratt et al., "Atypical 'beading' in the production of cultured pearls from Australian *Pinctada maxima*," *GIA Research News*, 2017, https://www.gia.edu/gia-news-research/atypical-beading-production-cultured-pearls-australian-pinctada-maxima), this is the first time the author has analyzed the detailed color origin of Sango pearls with

Pinctada fucata mollusks as the host. The pearls are known to possess relatively thin nacre overgrowth, which has enabled the creation of the commercial type of akoya cultured pearl using a natural coral nucleus. GIA would classify Sango pearls as atypical bead-cultured pearls.

Kazuko Saruwatari
GIA, Tokyo

Tektite with a large fluid inclusion. Tektites are a form of natural glass related to extraterrestrial impact. When a meteorite hits Earth's surface, the impact site is subjected to tremendous heat and pressure. This causes the rocks to instantly melt and quickly cool, creating a glass with a bulk composition similar to that of the original host rock. Only the most volatile elements will be removed, because their gaseous phases escape easily. This is the case for fluids and gases such as water and carbon dioxide, as well as certain metals. This melting and cooling results in a silica-dominated glass called tektite that is often very dark green to black.

Tektites are common in many parts of the world. The most famous type is probably moldavite, related to an impact in southern Germany. The world's largest tektite area is the Australasian field, which covers Australia (australites), southeast Asia (indochinites), and most of the Indian Ocean. It is related to a single impact 790,000 years ago, although the impact crater has not been identified.

The gem mines in northern Vietnam around Thac Ba Lake, which are famous for ruby and spinel, also yield tektite from secondary deposits. Local dealer Geir Atle Gussiås (BalderGems) procured a large tektite weighing 230.9 g (figure 13) with a very large fluid inclusion. The inclusion contained a mix of gas and liquid, which could be seen under strong illumination (figure 14; see video at http://www.gia.edu/gems-gemology/tektite-inclusion). GIA's Bangkok lab examined this unique piece by comparing it to six tektite samples collected in the mines during several field expeditions to Vietnam.

We examined the specimen and performed density measurements as well as chemical analysis to determine whether it was a real tektite. The surface features and overall shape of the large piece were very similar to the reference samples, although the reference samples were much smaller. The overall color was black, but when strong light was transmitted through the sample, a brown color was observed. The SG of the reference samples ranged from 2.01 to 2.42. This range can be explained by differences in chemical composition, mainly iron concentration, and the amount of gas bubbles in the matrix, which lowers the SG. The SG of the Vietnamese sample was 1.84, indicating an unusual abundance of fluid and/or gaseous inclusions in the sample. Because this tektite was too large to analyze using LA-ICP-MS, its chemical composition, along with those of the reference samples, was revealed with EDXRF. The large tektite had Fe, Sr, Rb, and Zr contents that are comparable to the other Vietnamese tektites.

Figure 13. A large tektite (230.9 g) from Luc Yen, Vietnam, surrounded by six tektite samples from the GIA reference collection. Photo by Wim Vertriest.

We then imaged the internal structure using real-time X-ray microradiography (RTX), a technique commonly used in pearl analysis. Because the device has a small detector, we could not view the whole tektite in one image. The maximum resolution of 4 µm should have been sufficient to pick up any artificial structures such as drill holes. The RTX images show the irregular outline of the tektite's surface and a large bubble with a smooth outline (figure 15). Several smaller negative inclusions are also visible as dark ovals. When the sample was moved under the RTX, the liquid-gas inclusion was clearly seen because of the motion of the liquid.

Since we did not find a drill hole or any signs of man-made glass, we assume that the liquid in the negative inclusion is a natural phenomenon. Since glass is not porous, it seems most likely that the liquid was included during the tektite's formation. Although this could not be proven, this tektite remains a unique specimen.

Wim Vertriest, Vararut Weeramonkhonlert, and Kwanreun Lawanwong
GIA, Bangkok

Figure 14. A close-up view of the tektite sample using very strong backlighting reveals a curved black line, which is the liquid-gas contact. Photo by Wim Vertriest.

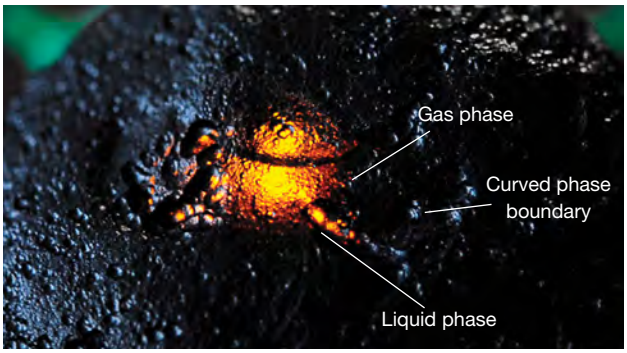

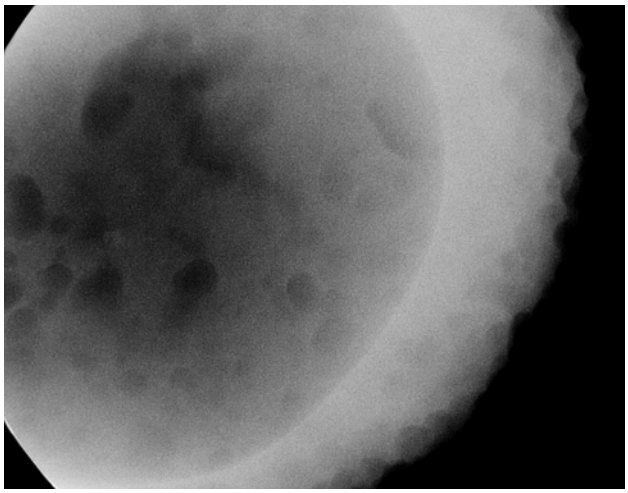

Figure 15. This RTX image shows the tektite's irregular outline on the right side. The very large negative inclusion has a smooth outline. Several other smaller negative pockets can also be seen.

SYNTHETICS AND SIMULANTS

Dyed yellow beaded freshwater cultured pearls imitating South Sea cultured pearls. In the spring of 2017, the Gübelin Gem Lab received a yellow pearl necklace for testing. The size and color of the specimens implied that they were South Sea cultured pearls. The high insurance value appeared to confirm this; however, there were some suspicious color patches that suggested the material had been dyed.

Only a few months earlier, author LK visited the Hong Kong office of Grace Pearls, a large producer with a pearl farm and factory in China, to see their latest batch of freshwater cultured pearls. Grace Pearls developed a proprietary method to grow large freshwater pearls with bead, marketed as "Edison" pearls. These occur in all the known colors of traditional freshwater pearls, typically white, orange, pink, and purple. To complement their color range, they also offer yellow and black treated pearls ranging from approximately 12 to 18 mm.

The goods we saw at Grace Pearls had a wide range of qualities and prices. The lowest price for a strand of Edison pearls was approximately US$100, while the highest-quality yellow dyed pearls go for as much as US$2,000. Prices for top-quality white and pink natural-color pearls may reach up to US$40,000 per strand.

The Gübelin Gem Lab acquired from Grace Pearls a necklace of yellow dyed freshwater bead-cultured pearls to complement our extensive reference collection. The largest of these pearls measured nearly 17 mm. For study purposes, we deliberately chose a low-quality necklace showing color concentrations, slightly irregular colors from pearl to pearl, and slight blemishes on the surface (figure 16).

The grafting process, which Grace Pearls considers a proprietary method, appears to be similar to that of "Kasumigaura pearls" from Japan and "Ming pearls" from China,

Figure 16. Uneven color and blemishes on the surface of a low-quality dyed cultured freshwater pearl necklace obtained from Grace Pearls. Photo by Lore Kiefert.

where the bead is drilled first and a tissue is partly inserted into the drill hole in order to introduce both tissue and bead at the same time during the implantation procedure (H.A. Hänni, "Ming pearls: A new type of cultured pearl from China," *Journal of the Gemmological Association of Hong Kong*, Vol. 32, 2011, pp. 23–24). X-ray images clearly show drill holes in the beads of several of these cultured pearls, mostly in the smaller beads (figure 17), while larger beads, like the one in the center of figure 16, have only one drill hole. This may be due to a possible re-implantation into the pearl sac once the first pearl has been harvested. X-ray fluorescence (XRF) analysis gave Mn and Sr values consistent with those of freshwater pearls.

Upon testing, the necklace submitted by the client showed identical properties: dark yellow color concentrations around drill holes and in cavities, uneven surfaces with various shades of yellow (figure 18, left; see also C.

Figure 17. X-ray image of yellow dyed freshwater cultured pearls. The beads range from approximately 10 to 15 mm in diameter, while nacre thickness varies from <0.2 to >5 mm. Some of the beads show an additional drill hole. Image by Pierre Hardy.

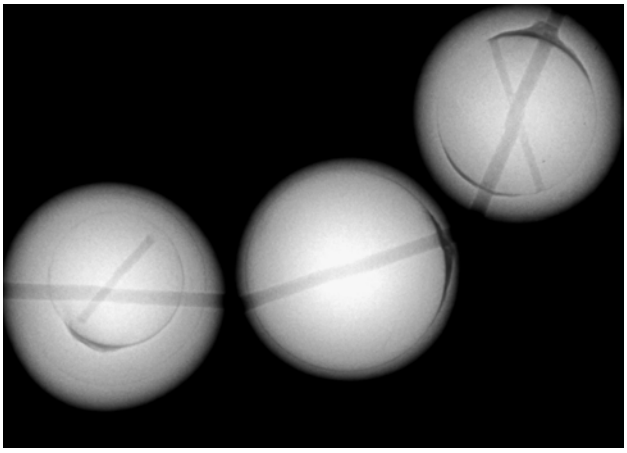

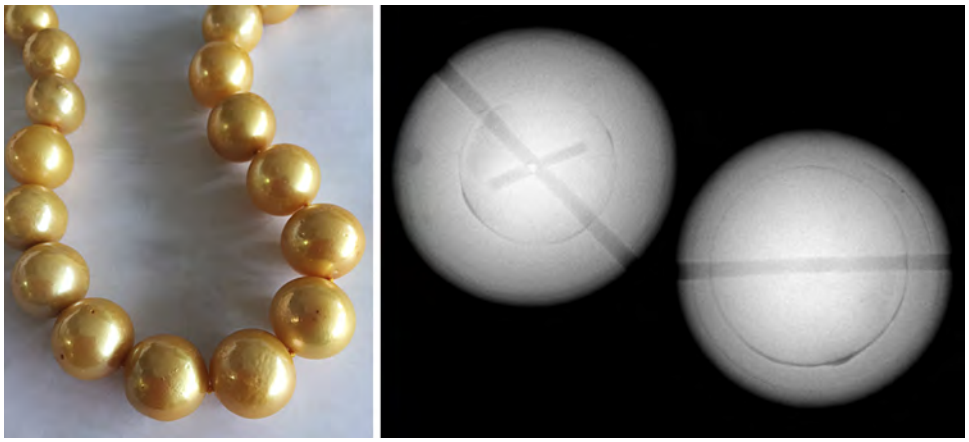

Figure 18. Left: Blemishes and dark color concentrations in cavities on the surface of dyed cultured freshwater pearls in a client-submitted necklace. Photo by Lore Kiefert. Right: An X-ray image of two pearls from the client necklace showing a clear bead. The left pearl displays an additional drill hole in the bead. Image by Pierre Hardy.

Zhou et al., "Update on the identification of dye treatment in yellow or 'golden' cultured pearls," Winter 2012 *G&G*, pp. 284–291), X-rays showing an additional drill hole through the bead in some of the pearls (figure 18, right), and the chemical composition of freshwater pearls (figure 19). This demonstrates the importance of staying informed on new developments in the market.

Lore Kiefert and Pierre Hardy
Gübelin Gem Lab
Lucerne, Switzerland

Figure 19. A plot showing the theoretical distribution of MnO vs. SrO in freshwater and saltwater pearls (after W. Gutmannsbauer and H.A. Hänni, "Structural and chemical investigations on shells and pearls of nacre forming salt- and fresh-water bivalve molluscs," Journal of Gemmology, Vol. 24, No. 4, 1994, pp. 241–252). The red dots represent values for our reference collection necklace, the yellow dots the values for the client-submitted necklace.

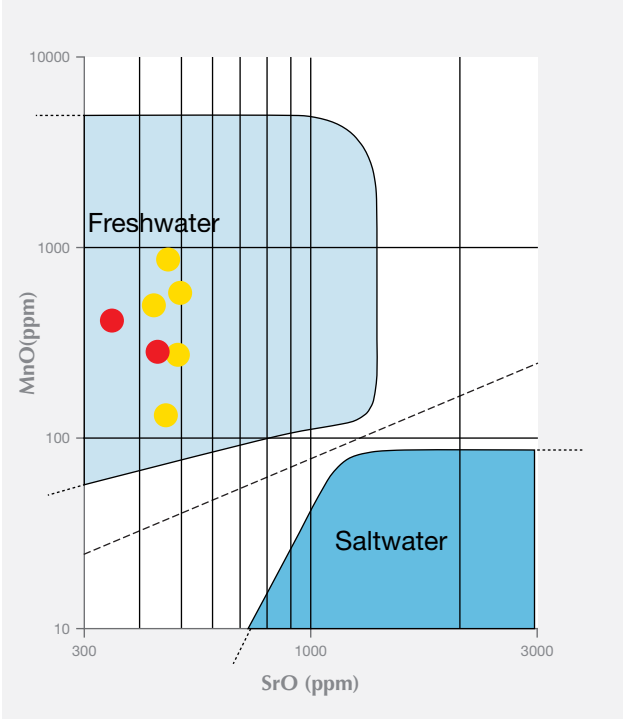

Colorful chatoyant glass. This year at the Tucson gem shows, this author encountered an interesting new product of chatoyant devitrified glass (glass that has converted to a crystalline material) marketed as "Starburst Stone." This material (figure 20) closely resembles the chatoyant glass known as Victoria Stone, which was developed in Japan by Dr. Satoyasu Iimori in the 1950s and produced for almost 40 years (http://victoriastone.sakura.ne.jp/JP-30-88-B.pdf).

John Bennett, in partnership with Artur Birkner (both based in Perth, Western Australia), began developing Starburst Stone in 2013, and this is the first year of commer-

Figure 20. Starburst Stone is a colorful new devitrified glass, reminiscent of the product once marketed as Victoria Stone. Photo by Kevin Schumacher; courtesy of Australian Rough and Tumble.

cially available production (approximately 100 kilograms). This devitrified glass is made from a chemical mixture that is cooled at a rate to facilitate nucleation and growth of dense networks of elongate lath-like crystals, and each batch of glass is colored by the addition of certain metals. Darker blues are achieved by adding cobalt, lighter blue by adding copper, and green by adding chromium to the glass mixture.

Standard gemological testing revealed properties consistent with manufactured glass. The RI was between 1.51 and 1.52 and varied slightly between the different colors tested. The average SG, measured hydrostatically, was 2.62. Raman analysis identified the devitrification product responsible for the chatoyancy as apatite, which was also responsible for the chatoyancy in the devitrified glass product known as Victoria stone.

Dark and light blue, green, and golden Starburst Stones are being manufactured, with additional colors in development. This new ornamental glass showing chatoyancy is a welcome addition to the gem trade. Those interested in the material once sold as Victoria Stone will certainly appreciate this very similar phenomenal glass product.

Nathan Renfro

TREATMENTS

Chalcedony beads coated with titanium nitride. Recently, RAG Gemological Laboratory in Turin received a necklace of unusual metallic appearance (figure 21). The beads showed irregular surfaces that were actually small geodes with shiny and well-shaped crystals. The cavities in the beads (figure 22) were reminiscent of the small quartz-lined holes that are often formed in agates and chalcedony. The necklace consisted of 29 beads ranging from 12.0 to 12.5 mm in diameter, with a total weight of 84 g.

Some loose opaque beads provided by the necklace's owner allowed us to measure the material's density. The value of 2.60 g/cm^3 was in agreement with chalcedony. RI was not measurable on the beads due to their rough surface. No fluorescence reaction was observed under long- or short-wave UV. A sawed bead revealed that the inner part consisted of light gray chalcedony without zonation (figure 23). Observation of the area near the drill holes showed discoloration and the true color of the underlying material. The coating on these grayish gold chalcedony beads in this necklace had an unusual composition. The unusual color and reflectivity of the external surface, clearly not inherent to chalcedony, warranted investigation.

The chemical composition of the bead was confirmed by energy-dispersive spectroscopy (EDS) using a Cambridge Stereoscan 360 scanning electron microscope equipped with an Oxford Inca Energy 200 EDS and a Pentafet detector for the determination of elements from boron to uranium. The results showed homogeneous composition on the sample surface, with titanium, oxygen, and silicon as major elements. No known compound of Ti and Si could explain the nature of the bead's surface or the goldish gray metallic tinge.

Figure 21. The beads in this necklace, ranging in diameter from 12.0 to 12.5 mm, have a submetallic luster and a gray tinge with goldish reflection. Small vugs lined with sparkling crystals are clearly visible in most of the beads. Photos by Raffaella Navone.

Low-acceleration voltage conditions in EDS analysis (4 kV) allowed us to enhance the X-ray emission yield of lighter elements and reduce the penetration depth of the electron beam at around 100 nm into the bead's surface. The EDS spectra at low acceleration voltage showed the presence of nitrogen and titanium, suggesting a coating of titanium nitride (TiN) on the beads. At low potential the electron beam could pass through the thin layer of TiN, so the oxygen and silicon peaks from the underlying silica were still visible in the spectra. We calculated the thickness of the coating by acquiring several EDS spectra at dif-

Figure 22. SEM imaging shows the small, well-shaped quartz crystals within the cavities. The crystal in the lower middle clearly displays the classic "flute" termination typical of quartz. Image by Emanuele Costa; field of view 1 mm.

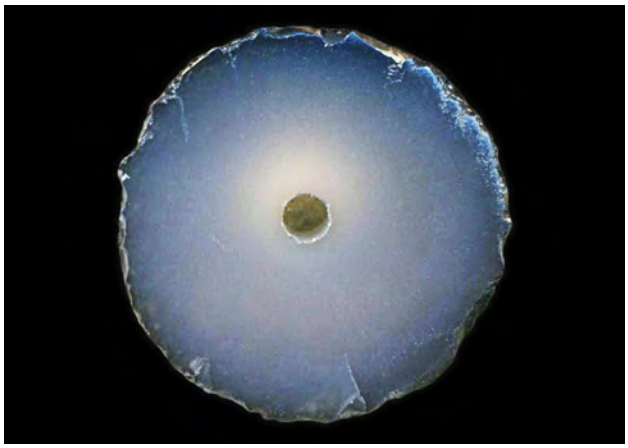

Figure 23. This sawed cross-section clearly demonstrates the homogeneity and light gray color of the chalcedony that constitutes most of the bead. Photo by Emanuele Costa.

ferent acceleration voltages (from 4 to 10 kV). The presence of the silicon peak even at 4 kV suggests that the electron beam could penetrate the layer and generate the signal through the TiN coat. The Casino software package evaluated the corresponding excitation depth of the electron beam using a Monte Carlo simulation. The calculated maximum thickness in our samples was less than 200 nm.

TiN is a very difficult material to analyze due to the presence of nitrogen, which is not always revealed with standard gemological techniques. To confirm the presence of a TiN film coating, we performed micro-Raman investigations. Spectra were obtained using a micro/macro Horiba LabRAM HR 800 (UV-Vis-IR) equipped with an Olympus microscope. The backscattered Raman signal was collected with a 50× objective and the 632.8 nm line of a He-Ne laser. The spectra were collected with multiple and repeated acquisitions to improve the signal-to-noise ratio, but even with these precautions the quality of the spectra is very poor due to the low intensity of Raman response from TiN. The Raman spectrum was recorded from 100 to 1200 cm^{-1}. Spectral manipulation such as baseline adjustment, smoothing, and normalization were performed using LabSpec 5 software. Band component analysis using the Fityk software package enabled the type of fitting function to be selected and specific parameters to be fixed or varied accordingly.

The Raman spectrum of a deposited TiN film is shown in figure 24. The Raman spectrum of the TiN layer can be fitted with Gaussian-Lorentzian peaks at 260, 330, 418, and 584 cm^{-1}. The spectrum is the same as those of TiN films reported, also with very poor quality, in the literature (Y.H. Cheng et al., "Substrate bias dependence of Raman spectra for TiN films deposited by filtered cathodic vacuum arc," *Journal of Applied Physics,* Vol. 92, 2002, pp. 1845–1849). Slight variations in peak position, shape, and relative intensity can be influenced by thickness (C.C. Chen et al., "Raman spectra of titanium nitride thin films," *Chinese Journal of Physics*, Vol. 32, No. 2, 1994, pp. 205–210), treatment time, and deposition temperature of TiN films (R.R.M. de Sousa et al., "Cathodic cage plasma deposition of TiN and TiO_2 thin films on silicon substrates," *Journal of Vacuum Science & Technology A, Vacuum, Surfaces and Films*, Vol. 33, No. 4, p. 041502), as well as substrate bias.

The TiN films also contained a small quantity of crystalline phase of TiO_2 (i.e., brookite) that was identified in the bead coating using Raman spectroscopy. There was a close match between the collected spectrum and that of brookite available in the RRUFF database (R050363). The association of TiN and TiO_2 films is well known and widely studied (de Sousa et al., 2015).

TiN deposition is widely used for the coating of small mechanical parts or tools, giving them a higher resistance to corrosion and scratching. Therefore, TiN films are essential for applications such as wear-resistant coatings, diffusion barriers, and optical coatings. The coating typically produces a golden hue, but other colors are also possible. Even though TiN films are common in industrial applications, this may be the first time such a coating has been reported in gemology.

Emanuele Costa and Erica Bittarello
Department of Earth Sciences, University of Turin
Raffaella Navone
RAG Gemological Laboratory, Turin

Figure 24. Raman spectrum of the TiN film in the 100–800 cm^{-1} region. The Raman bands are related to transverse acoustic (at 260 cm^{-1}), longitudinal acoustic (330 cm^{-1}), second-order acoustic (418 cm^{-1}), and transverse optical (584 cm^{-1}) modes of TiN, respectively (Cheng et al., 2002). The poor quality of the spectrum, despite a long collection time and enhanced sensitivity, is due to the faint response of the TiN to Raman investigation (as well as to the extreme thinness of the coating); it is comparable to the reported spectra available in the literature.

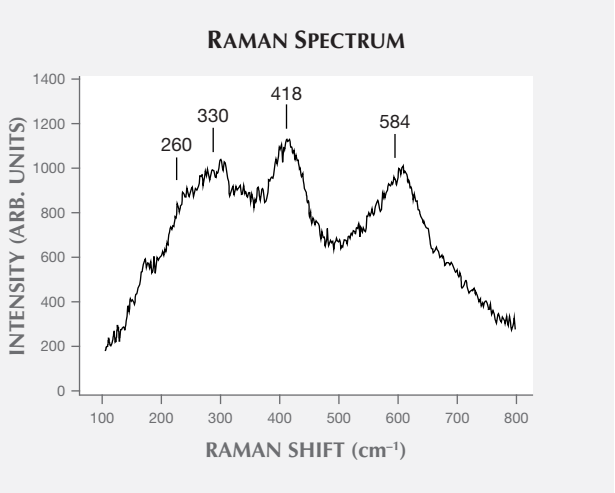

Figure 25. This 68 ct synthetic CZ shows three distinct hues in CIE standard illuminant F10 (left), CIE standard illuminant F9 (center), and CIE standard illuminant D65 (right). Photos by Robison McMurtry.

Tri-color-change holmium-doped synthetic CZ. Colored yttria-stabilized synthetic cubic zirconia (CZ) has been an attractive diamond substitute since the late 1970s (R.T. Liddicoat and J.I. Koivula, "Synthetic cubic stabilized zirconia," Summer 1978 *G&G*, pp. 58–60). The different colors seen in synthetic CZ are caused by the introduction of specific transition metal elements and rare earth elements (K. Nassau, "Cubic zirconia: an update," Spring 1981 *G&G*, pp. 9–19). At this year's Tucson Gem and Mineral Show, the authors obtained an interesting synthetic CZ rough that exhibited an unusual color-change behavior (figure 25). Unlike traditional color-change stones such as alexandrite, color-change corundum, and color-change garnet, this material did not exhibit different colors when illumination alternated between incandescent light and daylight conditions (approximated by CIE standard illuminants A and D65, respectively). Surprisingly, it showed three distinct hues in daylight/incandescent light (yellowish green), in fluorescent lighting corresponding to CIE standard illuminant F9 (green-blue), and in CIE standard illuminant F10 (purplish violet). One wafer with 3.32 mm thickness was polished and analyzed to understand this color-change phenomenon.

The wafer's chemical composition was obtained using a Thermo Fisher iCAP Q ICP-MS coupled with a New Wave Research UP-213 laser ablation unit. LA-ICP-MS analyses were performed in the same spot where the spectroscopic data was collected. Based on its calculated chemical formula of $Zr_{0.52}Y_{0.45}Ho_{0.02}Hf_{0.01}O_{1.79}$ (the formula is nonstoichiometric and calculated by forcing cations to 1 atom per formula), the wafer was a holmium-doped yttria-stabilized CZ (S. Gutzov et al., "High temperature optical spectroscopy of cubic holmium doped zirconia, $Zr_{0.78}Y_{0.21}Ho_{0.01}O_{1.90}$," *Physical Chemistry Chemical Physics*, Vol. 9, No, 4, 2007, pp. 491–496). Holmium was the only detected chromophore, at a concentration of about 7780 ppma.

Visible spectra were collected with a Hitachi U-2910 spectrometer with a 1 nm spectral resolution at a scan speed of 400 nm/min. The wafer's spectrum matched the holmium-doped CZ spectrum reported by Gutzov et al. (2007). The unusual color change under different illuminants can be qualitatively understood by examining figure 26. The violet and orange emission peaks of the F10 illuminant are not absorbed by Ho-doped CZ; however, there is significant absorption by holmium of the green emission peak for the F10 illuminant. This selective absorption of the F10 emissions creates a purplish violet color (figure 26, top). The F9 illuminant has more of a broadband emission,

Figure 26. The UV-Vis-NIR absorption spectrum of holmium-doped synthetic CZ is shown with the relative power distribution curves of CIE illuminant F10 (top), CIE illuminant F9 (middle), and CIE illuminant D65 (bottom).

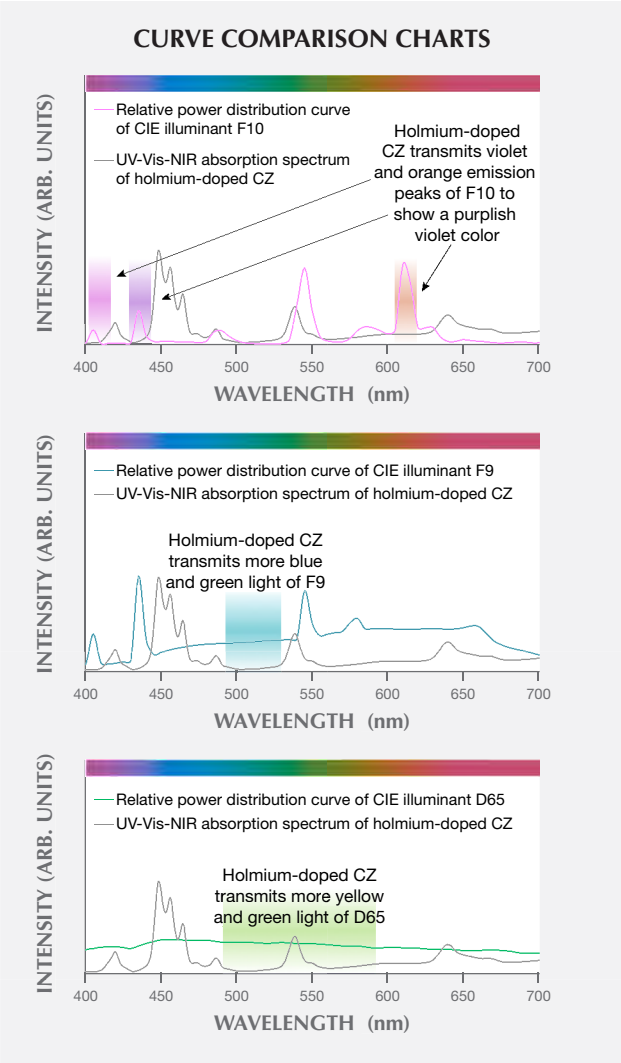

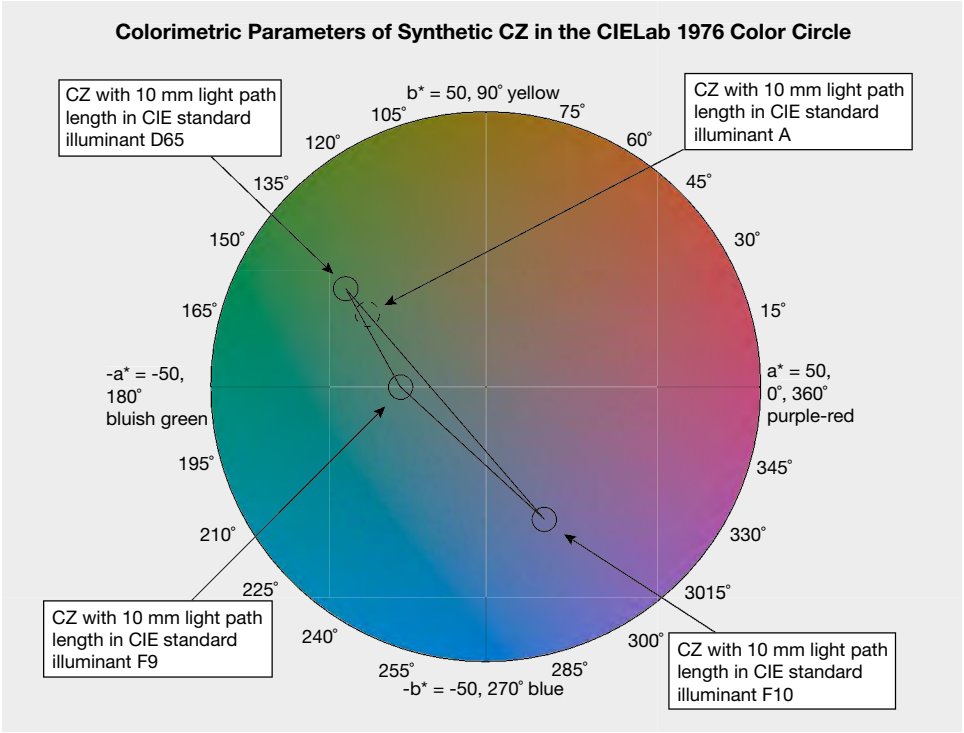

Figure 27. In the CIELab 1976 color circle, the color of holmium-doped synthetic CZ with 10 mm light path length changes from yellowish green in CIE standard illuminant D65 to blue-green in CIE standard illuminant F9 to purplish violet in CIE standard illuminant F10. The hue angle differences are 148.61° between D65 and F10, 34.96° between D65 and F9, and 113.65° between F10 and F9. The chroma differences are 4.73 between D65 and F10, 15.52 between D65 and F9, and 10.79 between F10 and F9. In contrast, the hue angle difference and chroma difference between D65 and A are 3.37° and 5.79, respectively.

which is unaffected by the strong but narrow absorption by holmium of green light at 540 nm. This results in a blue-green color under F9 illumination (figure 26, middle). The D65 illuminant is essentially a broadband emission roughly corresponding to a black body irradiator at 6500 K. Under D65 illumination, a yellowish green color is produced because of the strong absorption of blue light by holmium (figure 26, bottom).

The wafer's visible absorption spectrum was reflection-corrected by subtracting the absorbance value at 850 nm, where no chromophoric absorption is expected, from values for every other data point along the rest of the spectrum. The reflection-loss-corrected visible spectrum can then be used to quantitatively calculate the color of this material at a wide range of path lengths and under different lighting conditions (Z. Sun et al., "Vanadium- and chromium-bearing pink pyrope garnet: Characterization and quantitative colorimetric analysis," Winter 2015 *G&G*, pp. 348–369). There are large differences in the CIE L*, a*, b* color coordinates between D65, F10, and F9 (figure 27). One way to judge the quality of a color-change stone is to plot the color pair in the CIE 1976 color circle. Well-defined color-change pairings show a large hue angle difference, a small chroma difference, and high chroma values. The color coordinates of the material with a 10 mm light path length in D65, F9, and F10 were plotted in the CIE 1976 color circle shown in figure 27; calculated color panels for the illuminants were also placed alongside the faceted material (see online at http://www.gia.edu/gems-gemology/summer-2017-gemnews-holmium-synthetic-cz). The fact that the material shows three distinct hues in three different white lights makes it unique.

Ziyin Sun and Nathan Renfro
Aaron C. Palke
University of Queensland and Queensland Museum
Brisbane, Australia

ERRATA

1. The cover description on the Spring 2017 masthead page was incorrect. The cover photo actually shows a rose-cut diamond brooch, or "stomacher," from France that contains over 10 carats of diamonds set in silver over gold. It has a 1.90 ct center stone and three side stones totaling 5.05 ct. The photo is by Robert Weldon, courtesy of Lang Antique & Estate Jewelry (San Francisco, California).

2. In the Spring 2017 Gem News International section, the cultured pearl market update (pp. 124–126) showed a necklace featuring baroque South Sea cultured pearls (figure 23), which the caption described as "keshi." We would like to clarify that these are baroque, beaded (bead-cultured) pearls and cannot be true keshi pearls, which are pearls produced by a loose tissue piece, or in a pearl sac that previously held a bead or cultured pearl. We are grateful to Prof. Henry A. Hänni for this observation.